Synthesis, characterization, and photocatalytic properties of core/shell mesoporous silica nanospheres supporting nanocrystalline titania

**K. Cendrowski · X. Chen · B. Zielinska ·
R. J. Kalenczuk · M. H. Rümmeli ·
B. Büchner · R. Klingeler · E. Borowiak-Palen**

Abstract The facile bulk synthesis of silica nanospheres makes them an attractive support for the transport of chemical compounds such as nanocrystalline titanium dioxide. In this contribution we present a promising route for the synthesis of mesoporous silica nanospheres (m-SiO$_2$) with diameter in range 200 nm, which are ideal supports for nanocrystalline titanium dioxide (TiO$_2$). The detailed microscopic and spectroscopic characterizations of core/shell structure (m-SiO$_2$/TiO$_2$) were conducted. Moreover, the photocatalytic potential of the nanostructures was investigated via phenol decomposition and hydrogen generation. A clear enhancement of photoactivity in both reactions as compared to commercial TiO$_2$-Degussa P25 catalyst is detected.

K. Cendrowski · X. Chen · B. Zielinska ·
R. J. Kalenczuk · E. Borowiak-Palen (✉)
Centre of Knowledge Based Nanomaterials and Technologies, Institute of Chemical and Environment Engineering, West Pomeranian University of Technology, Szczecin, Poland
e-mail: eborowiak@zut.edu.pl

M. H. Rümmeli · B. Büchner
Leibniz Institute for Solid State and Materials Research Dresden, 01171 Dresden, Germany

M. H. Rümmeli
Technische Universität Dresden,
01062 Dresden, Germany

R. Klingeler
Kichhoff-Institute for Physics, Heidelberg University, Heidelberg, Germany

Introduction

The coating of nanoparticles surfaces with materials to form core/shell structures is an active research field. This is due to the fact that coating allows modification and tailoring of key physical and chemical properties. In addition, core/shell nanoparticles are predicted to exhibit novel properties that differ to those present in either the core or the shell materials (Das et al. 2007; Le et al. 2007).

Silica nanospheres are commonly used as a core material to host guest shell structures (Lim et al. 2008). The first study on the synthesis of silica nanospheres was conducted by W. Stöber and others in the 1970s (Stober et al. 1968). Due to the simplicity of this method (the Stober method) it became the leading route of the preparation of silica spheres. This synthesis route is based on the hydrolysis of a silica precursor in an alcohol–ammonia solution. Various improvements and modifications have been applied to the initial Stober route (Chen 1998). Similar methods of synthesis of silica shell

around iron oxide (Deng et al. 2008) and carbon core (Jia et al. 2007; Bian et al. 2009) have been also investigated. In comparison to other recently described techniques, this method requires mild conditions and short process time (Yang et al. 2008). For example, Zhang et al. and Jin Zhang et al. described the synthesis routes of core/shell structure based on harsh conditions such as microwave-assisted solvothermal methods or laser irradiation, respectively (Zhang et al. 2008, 2006). Therefore, the proposed synthesis of silica/titania core/shell structure is considered to be simple and the produced material exhibits high degree of uniformity in shape/size and purity in a bulk scale.

The convenience and high controllability of this synthesis route along with the ease with which one can modify the structural and chemical properties of silica nanospheres make them highly attractive as building blocks for the tailored formation of capsules or porous structures for chemical transport applications, viz. one can load the nanoparticles. Furthermore, the low toxicity of silica is advantageous in many potential applications (Zhu et al. 2010; Park et al. 2009).

In this study, we fabricate mesoporous silica nanospheres (m-SiO$_2$) which serve as an excellent support for nanocrystalline titanium dioxide (TiO$_2$) resulting in a core/shell structure (m-SiO$_2$/TiO$_2$). Additional studies to investigate their photocatalytic activity for water purification and hydrogen generation were conducted. Comparative photocatalytic studies were performed with TiO$_2$-Degussa P25 (a widely used and commercially available catalyst). Titanium dioxide has been intensively explored as a semiconductor photocatalyst since Fujishima and Honda discovered the photocatalytic splitting of water on TiO$_2$ electrodes in 1972 (Fujishima and Honda 1972). Recently, the use of TiO$_2$ has mainly concentrated on the decomposition of toxic and hazardous organic pollutants in contaminated water/air, which is of great importance for the environmental protection (Muruganandham and Swaminathan 2006; Tan et al. 2010; Fei et al. 2007; Park et al. 2006). However, the correlation between the photocatalytic activity of TiO$_2$ particles and their mean size and shape is still widely discussed (Tian et al. 2006). Here, we tested the photocatalytic activity of titania coating ($\sim$2–5 nm in thickness) supported on mesoporous silica via two experiments, namely, phenol

decomposition and hydrogen generation. The presence of a mesoporous silica structure enabled their efficient and homogeneous coating with titania (anatase phase).

Experimental section

Synthesis of silica nanospheres (SiO$_2$)

1.5 mL tetraethyl orthosilicate (TEOS) and 50.0 mL ethanol (EtOH) were mixed together in a reactor and refluxed. After careful mixing at 64 °C, 2.5 mL of ammonium (NH$_3$·H$_2$O) was added. The resultant mixture was stirred for 18 h. The suspension was centrifuged at 8,000 rpm for 10 min and the sediment was washed with ethanol and centrifuged again.

Synthesis of mesoporous silica nanospheres (m-SiO$_2$)

In order to create a mesoporous external layer on the as-produced silica spheres, first, a mixture of 0.5 g hexadecyl(trimethyl)azanium bromide (CTAB); 0.5 g NH$_3$·H$_2$O; 30 mL EtOH and 40 mL H$_2$O was prepared. After 30 min of stirring, 0.1 mL TEOS and 0.1 g silica nanospheres were added and the mixture was stirred for a further 18 h. The mixture was then centrifuged at 8,000 rpm for 10 min. In the next step the silica nanospheres were thoroughly washed with ethanol. In order to remove the surfactant the sample was annealed in air at 600 °C for 5 h.

Titania coating of mesoporous silica nanospheres (m-SiO$_2$/TiO$_2$)

To coat the mesoporous silica nanospheres a 10% solution of tetrabutyl titanate (TBT) was used as the TiO$_2$ source; 1 mL of TBT was add to 9 mL of ethanol and stirred for an hour. Next, this solution was mixed with the mesoporous silica spheres with different ratios and further mixed with ethanol (ratio 1:4) and stirred for 16 h. The suspension was then centrifuged (8,000 rpm for 10 min). In order to remove excess of titanium dioxide the sample was stirred with ethanol for 2 h and then treated ultrasonically for 1 h. This purification step was performed multiple times. Finally, the sample was heated with air flow at 600 °C for 2 h to transform

the titanium dioxide into its anatase phase which is active in photocatalytic reactions.

The experimental steps are depicted schematically in Fig. 1a–c

Determination of photocatalytic activity of m-SiO$_2$/TiO$_2$

The activity of m-SiO$_2$/TiO$_2$ was examined via the photocatalytic decomposition of phenol and hydrogen generation. Both reactions were carried out in an inner-irradiation-type reactor. A mercury lamp of 150 W was used as the light source. In both reactions the loading of Ti in the catalysts (m-SiO$_2$/TiO$_2$ and TiO$_2$-Degussa P25) was the same.

For the reaction of photocatalytic phenol decomposition, 700 cm^3 of phenol solution (initial concentration: 50 mg/dm^3) and the appropriate mass of the catalyst (m-SiO$_2$/TiO$_2$ or TiO$_2$-Degussa P25) were placed in the photoreactor. The mixture was continuously stirred during the experiment. After 30 min of adsorption in darkness, the reaction mixture was irradiated. Doses of the reaction mixtures were extracted at regular time intervals to determine the phenol concentration of the solution. The evaluation of phenol concentration was measured using a UV–Vis spectrophotometer (Jasco, Japan).

The photocatalytic hydrogen generation was examined in the presence of formic acid in a closed system. First, the photocatalyst powders were dispersed in 600 cm^3 of aqueous solution of formic acid (initial concentration: 0.1 mol/dm^3). Afterward, the suspension was mixed with assistance of a magnetic stirrer for 1 h, and during this time argon was passed through the reaction mixture to remove oxygen. Finally, the solution was irradiated for 3 h without argon purging. The amount of evolved hydrogen was determined using a gas chromatograph (Thermal conductivity detector, Ar as a gas carrier, model: Chrome5).

Characterization techniques

In order to study the morphology and chemical composition of the samples a transmission electron microscope Fei Tecnai G^2 F20 S Twin with energy dispersive X-ray spectroscopy as its mode were employed, respectively. Crystallographic phase identification of the samples was performed using X'Pert philips PRO X-ray diffractometer (X'Pert PRO philips diffractometer, CoK$_\alpha$ radiation). The vibronic properties were measured using a Renishaw InVia Raman spectroscope (excitation $\lambda = 785$ nm). Specific surface area analyzed through adsorption using
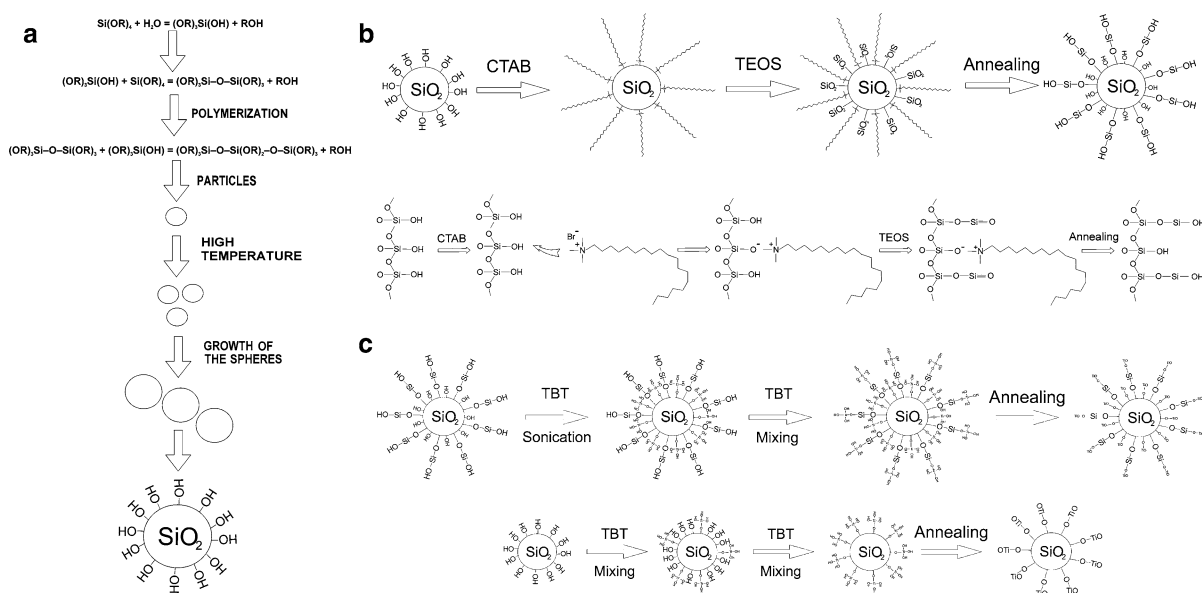

Fig. 1 Schemes of: **a** Synthesis of silica spheres, **b** Synthesis of mesoporous layer in silica nanospheres (m-SiO$_2$), and **c** Preparation of titania coating of mesoporous silica (m-SiO$_2$/TiO$_2$)

the Brunauer, Emmett and Teller (BET) isotherm was performed with a Quadrosorb SI (Quantachrome Instruments). The optical properties of the materials were investigated by means of diffuse reflectance (DR) UV–Vis technique using Jasco V-650 (Japan) spectrophotometer.
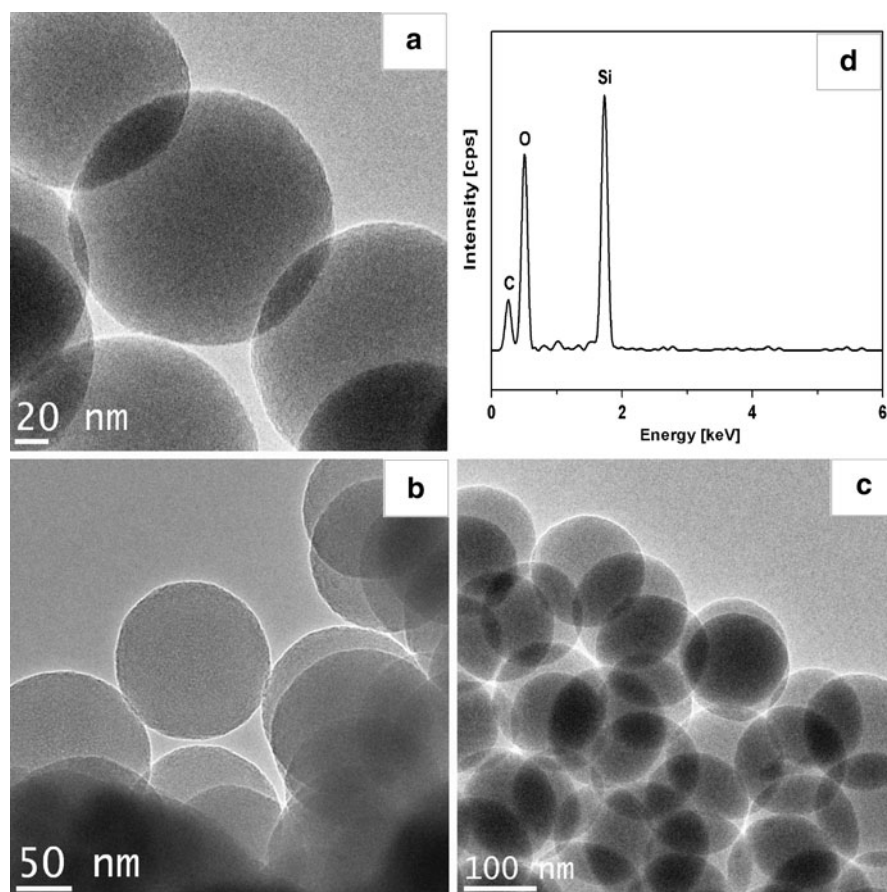
Results and discussion

The main aim of this contribution is the preparation of mesoporous silica nanospheres (m-SiO$_2$) used as support for nanocrystalline titanium dioxide (TiO$_2$) formed with a narrow diameter distribution and high purity. In order to achieve this, the first step is to optimize the synthesis of the starting solid silica spheres. Detailed TEM studies on the material indicated that the mean diameter of the nanospheres, their diameter distribution and tendency to agglomerate are strongly correlated to the experimental

parameters, namely, the mixing technique (magnetic stirrer or ultrasonication) and a process temperature. The morphology of the resulting product was sensitive even to the continuity of the solution stirring. When the solution was not continuously stirred the nanospheres were irregular in shape and easily formed agglomerates. The temperature of the process strongly influenced the mean diameter of the silica nanospheres. Higher temperature of the process resulted in the preparation of silica spheres with lower mean diameter. It was already investigated elsewhere that more energy delivered through increase of the temperature influences the reaction rate and more nuclei particles are formed (Lee et al. 2007). As a consequence this leads to the preparation of higher number of silica spheres with smaller diameter.

In our studies we used silica nanospheres produced at 64 °C with continuous magnetic stirring for 18 h. Figure 2 presents TEM micrographs of these spheres.

Fig. 2 TEM images of solid silica nanospheres (a–c); EDX spectrum of silica nanospheres (d)

Statistical analysis of the nanostructures revealed a mean diameter of 150 nm with the diameter distribution ranging between 130 and 170 nm. The EDX spectrum presented in panel d of this figure confirms the chemical composition of the sample to comprise Si and O. The carbon signal stems from the holey carbon TEM grid.

In the next step the formation of a mesoporous layer in the outer surface of the silica nanospheres was optimized. The treatment of silica nanospheres and TEOS using a mixture of CTAB; $NH_3 \cdot H_2O$; ethanol and 40 mL H_2O resulted in the formation of the mesoporous structure on the spheres. The thickness of the mesoporous layer varied between 65 and 85 nm (shown in Fig. 3). This layer can be clearly observed in TEM images of this material as a lighter contrast ring around the individual nanosphere. In addition, Fig. 3d presents the EDX spectrum of the sample and proves that the chemical composition of the sample remained unchanged. The additional

evidence for the successful formation of a mesoporous structure was provided by surface area measurements using the BET isotherm. The surface area increased from 26.15 to 987.01 m^2/g in the case of solid SiO_2 nanospheres and m-SiO_2, respectively.

Finally, the m-SiO_2 was used as a support for TiO_2 shell formation.

The key parameters in homogeneous coating of mesoporous silica nanospheres with TiO_2 are following: (i) the concentration of TBT, (ii) molar ratio of TBT to silica, (iii) time of the coating process. The silica spheres are coated efficiently when 10% solution of TBT is used. This allows to avoid the excess of titanium dioxide. The optimal ratio of m-SiO_2:TBT was evaluated to be 1.0:0.25, correspondingly. The coating was optimal when the process lasted 16 h. The shorter time did not lead to the desired effect of the homogenous TiO_2 layer. The morphology of this coated sample is shown in Fig. 4a–c. The presence of the mesoporous surface

Fig. 3 TEM images of mesoporous silica nanospheres (a–c); EDX spectrum of mesoporous silica nanospheres (d)
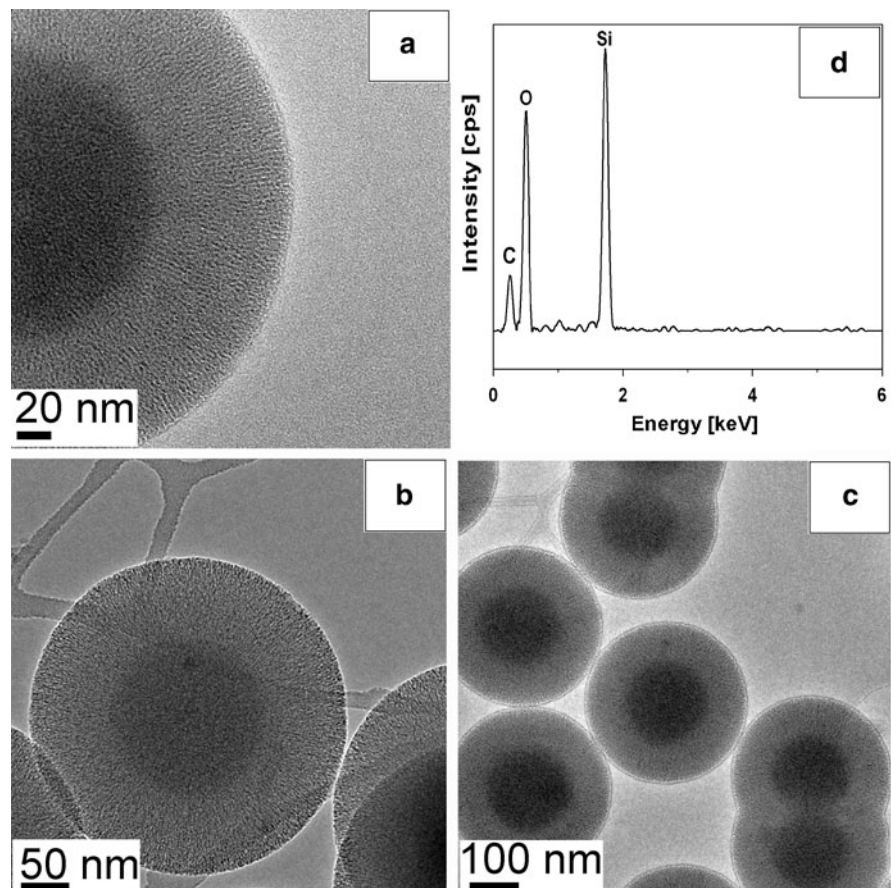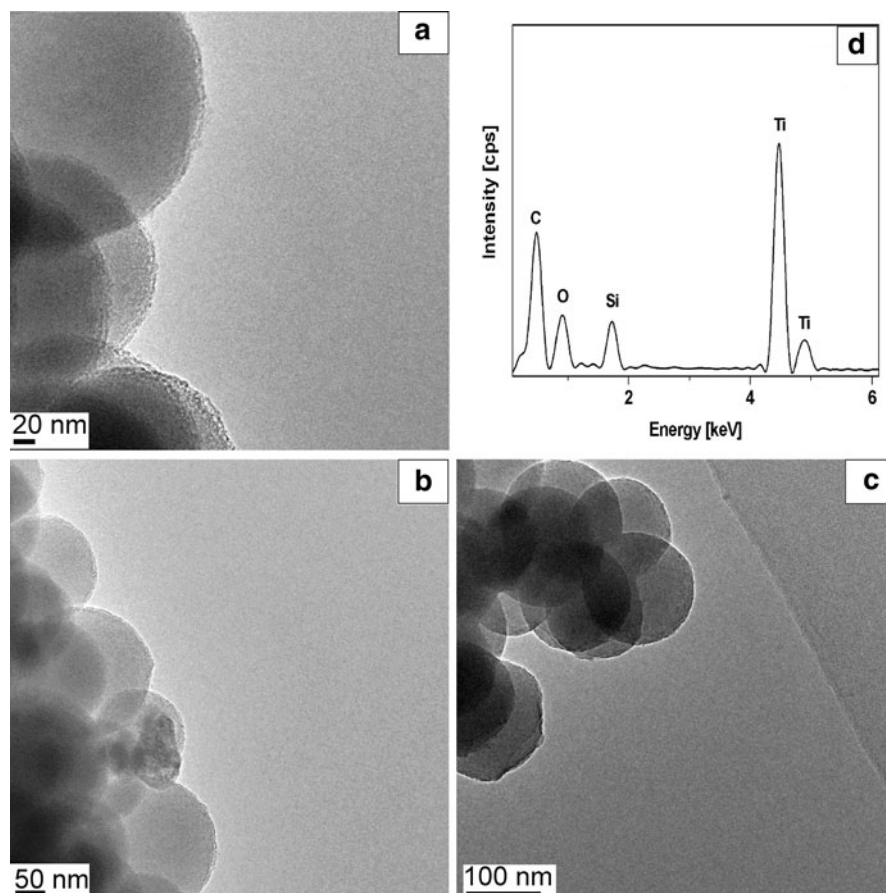
Fig. 4 TEM images of mesoporous silica nanospheres coated with titanium dioxide (**a–c**); EDX spectrum of coated mesoporous silica nanospheres (**d**)

on SiO_2 nanospheres makes the coating process much more efficient. This is due to the channels in the mesoporous shell which are not present in solid silica nanospheres. EDX studies confirmed the elemental composition of the TiO_2 coated mesoporous Si structures (see Fig. 4d). In order to quantify the amount of TiO_2 on m-SiO_2 surface the systematic EDX analysis of was preformed. Finally, it was calculated that there is 52.3 wt% of TiO_2 on m-SiO_2/TiO_2 after coating. BET surface area measurements showed a reduction from 987 to 157 m^2/g for m-SiO_2 and m-SiO_2/TiO_2, correspondingly. This indicates the partial filling and/or blocking of the mesoporous channels by the TiO_2.

In the case of untreated SiO_2 nanospheres the coating process had to be repeated at least six times so as to coat the spheres homogeneously but still the sample contained impurities (free titania nanocrystals) and it was difficult to control the diameter distribution of the sample. Figure 5 presents TEM images of untreated SiO_2 nanospheres coated two, four, and six times, respectively.

The crystallographic composition of the samples m-SiO_2 and m-SiO_2/TiO_2 was studied via XRD (Fig. 6). The diffraction pattern of m-SiO_2 shows two peaks: broad peak centered at $\sim$22.5 2θ assigned to the amorphous silica and sharp peak at $\sim$2.4 2θ arising from mesoporous (Chen et al. 2008). m-SiO_2 Diffraction pattern shows five peaks corresponding to the presence of TiO_2 in anatase phase and broad peak corresponding to the amorphous silica. In addition, the intensity of the peak assigned to mesopores significantly decreased proving efficient coating by TiO_2. XRD of the reference TiO_2-Degussa P25 proves that sample is composed of phase mixture (anatase and rutile) as indicated in the inset of Fig. 6.

The meso-porosity of mesoporous silica spheres and the mesoporous silica spheres supported with TiO_2 nanoparticles were revealed analyzed by N_2 adsorptoin–desorption measurements (see Fig. 7).
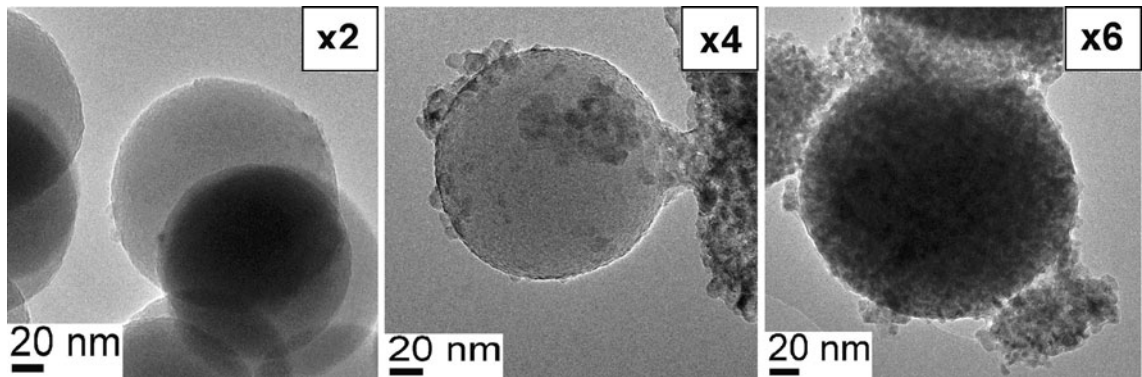
Fig. 5 TEM images of untreated silica nanospheres coated with titanium dioxide. Coating process repeated two, four, and six times (indicated in the insets)
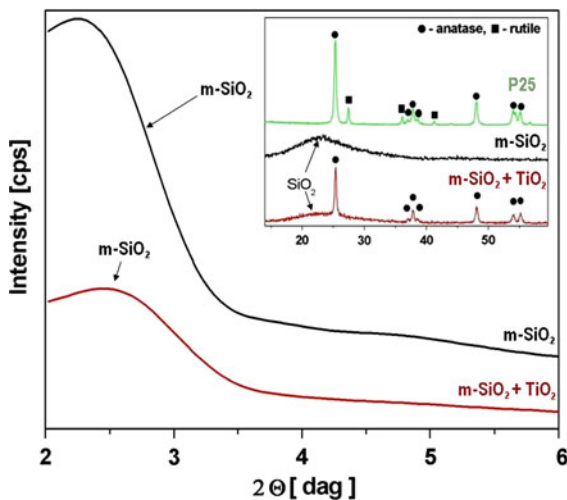

Fig. 6 XRD patterns of mesopores present in silica nanospheres (*black line*) and in mesoporous silica nanospheres coated with TiO$_2$ (*red line*). The inset shows full range XRD of reference P25 (*green line*); m-SiO$_2$–silica; m-SiO$_2$/TiO$_2$

Fig. 7 Isotherms of mesoporous silica nanospheres and mesoporous silica nanospheres coated with titanium dioxide

The shape of the isotherms are of typical IV with a hysteresis loop, representative of mesoporosity based on the IUPAC nomenclature. Considering the geometry of mesoporous silica spheres, they are assumed to contain cylindrical pores and no pore networks, thus satisfying to main requirements of the BJH method. The above results suggest that the core–shell structure silica spheres contain abundance of mesopores. From Fig. 7, the total surface area was calculated to be 967 m^2/g. When TiO$_2$ nanopaticles were deposited on mesoporous silica spheres the total surface area of m-SiO$_2$/TiO$_2$ decreased was estimated to be 157 m^2/g. Clearly, part of the mesopores of
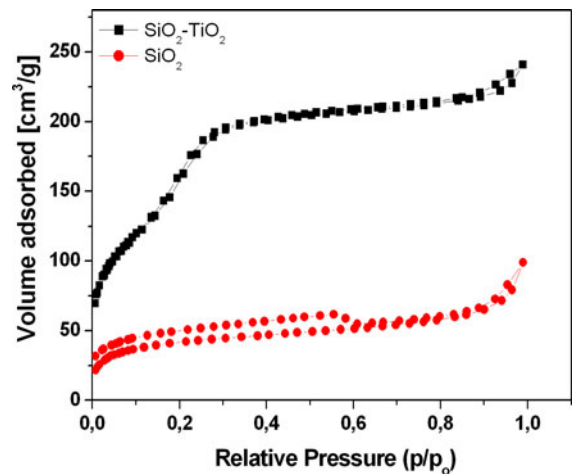
silica spheres has been occupied by TiO$_2$ nanoparticles. This result is consistent with XRD and TEM measurements.

Next, the samples were investigated by means of Raman spectroscopy. Figure 8 shows the Raman spectra of the starting solid silica nanospheres (black line), m-SiO$_2$ (gray line) and the final m-SiO$_2$/TiO$_2$ core/shell structure (red line). In the case of pure silica structures their Raman spectra are dominated by three spectral regions. The peaks below 400 cm^{-1} originate from torsional vibrations and O–Si–O bending modes. The strongest band in the range of 440–530 cm^{-1}, involves motions of O in Si–O–Si symmetric stretching–bending modes. The peaks above 600 cm^{-1} are correlated to Si–O stretching
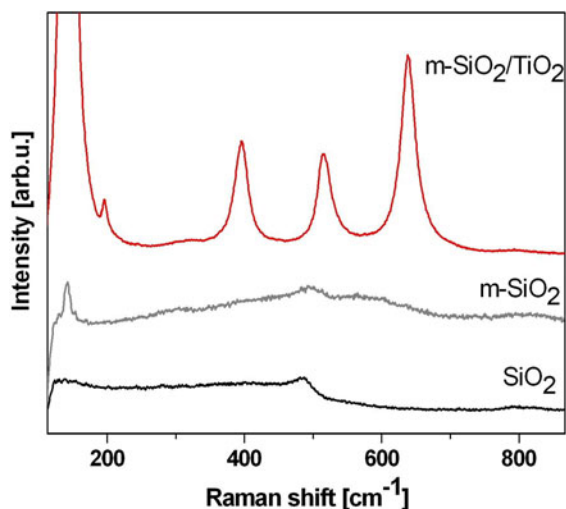
Fig. 8 Raman spectra of solid silica nanospheres (*black line*), mesoporous silica spheres (*gray line*), and core/shell structure of TiO_2 and SiO_2 (*red line*). The spectra measured with a 785 nm laser length

modes (Kingam and Hemley 1994). However, the Raman response of m-SiO_2/TiO_2 is strongly dominated by five peaks (142, 195, 396, 516, 639 cm^{-1}) corresponding to phonon modes from anatasa—a tetragonal phase of titania (Li et al. 2008). This confirms the efficiency of anatas phase coating. This is crucial because the anatase phase is significantly more photocatalytically active than the rutile phase.

To determine the photocatalytic activity of the synthesized m-SiO_2/TiO_2, the photocatalytic phenol decomposition and hydrogen evolution was investigated. The m-SiO_2/TiO_2 was compared to equivalent studies with commercial TiO_2-Degussa P25. The photocatalytic reactions were investigated with 191 mg of m-SiO_2/TiO_2 and 100 mg of TiO_2-Degussa P25. The Ti loading in both samples was the same. The mass of the photocatalysts for the process was estimated basing on EDX analysis provided above. The results of photocatalytic phenol decomposition and hydrogen generation are shown in Fig. 9a and b, respectively. Figure 9a shows a plot of C/C_0 versus time (t), where, C is concentration of the phenol at the certain time and C_0 is initial concentration of phenol (mg/dm^3). Figure 9b shows that the kinetics of hydrogen generation in the presence of formic acid during the first 3 h of UV

irradiation can be described by zero order kinetics. The presented results (see Fig. 9a and b) clearly indicate that the synthesized m-SiO_2/TiO_2 is active photocatalyst in phenol decomposition and hydrogen generation. In addition, it is more efficient than TiO_2-Degussa P25 in both processes. For example, in the reaction of phenol decomposition, after 180 min of UV irradiation, 100% and only 70% of phenol decomposition was obtained for m-SiO_2/TiO_2 and TiO_2-Degussa P25, respectively. Moreover, the rate constant of the hydrogen evolution over m-SiO_2/TiO_2 (0.94 mol H_2/min) is about 2.5 times higher than that of TiO_2-Degussa P25 (0.37 mol H_2/min). The obtained data confirm the argument that higher surface area results in higher catalytic photoactivity (Kim et al. 2007; Deng et al. 2002).

To estimate the band gap energy of the studied samples the optical analysis was conducted. The DR-UV–Vis spectra of TiO_2-Degussa P25, m-SiO_2/TiO_2, and m-SiO_2 are presented in Fig. 10. As shown in this figure, pristine m-SiO_2 hardly absorbs UV light. Spectra of TiO_2-Degussa P25 and m-SiO_2/TiO_2 reveal enhanced UV absorption edge at ~400 and 380 nm, respectively. The absorption edge of m-SiO_2/TiO_2 is shifted toward the shorter wavelength in respect to TiO_2-Degussa P25. To determine the band gap energy of TiO_2-Degussa P25 and m-SiO_2/TiO_2, the Kubelka–Munk method based on the DR spectra was employed. The experimental details were given elsewhere (Zielinska et al. 2011). The calculated band gap energy of TiO_2-Degussa P25 and m-SiO_2/TiO_2 is 3.05 and 3.30 eV, respectively. The increase of the band gap of m-SiO_2/TiO_2 can be due to the fact that TiO_2-Degussa P25 is composed of the anatase (~80% with band gap of ~3.2 eV) and rutile (~20% with band gap of ~3.0 eV) (Long et al. 2009; Wan et al. 2007). XRD pattern shown in Fig. 6 clearly indicates that TiO_2 in m-SiO_2/TiO_2 corresponds only to anatase. Therefore, this material with higher value of the energy band gap exhibits enhanced photoactivity in the studied model reactions (Yu et al. 2007).

Our preliminary result indicates that m-SiO_2/TiO_2 is a grate candidate for photocatalytic organic contaminant decomposition and hydrogen evolution. In addition, the material can be further modified with guest molecules, e.g., with Pt, in order to enhance the photocatalytic properties.

Fig. 9 The photocatalytic phenol decomposition (**a**) and hydrogen generation (**b**) over m-SiO$_2$/TiO$_2$ and TiO$_2$-Degussa P25 catalysts (phenol concentration– 50 mg/dm^3, HCOOH concentration–0.1 mol/dm^3)
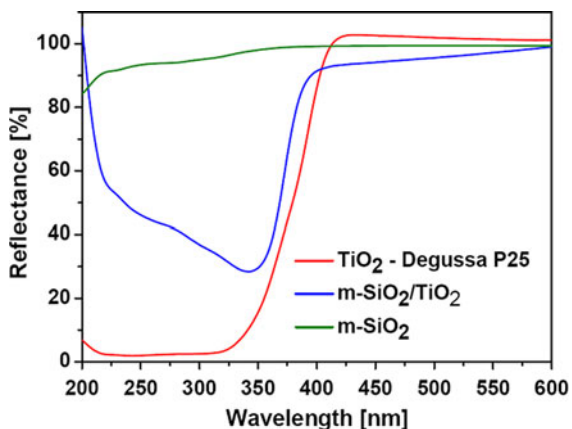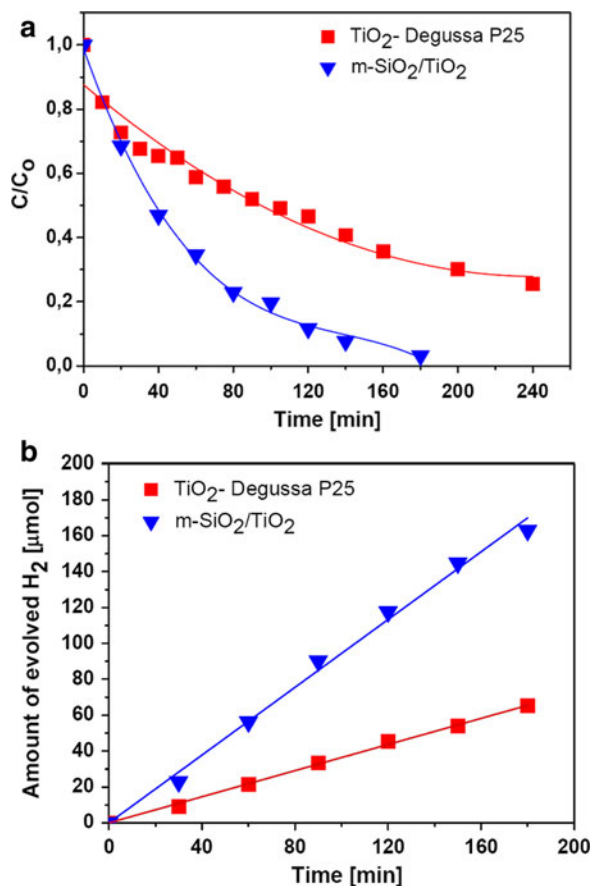

Fig. 10 DR-UV–Vis spectra of studied materials (TiO$_2$-Degussa P25, m-SiO$_2$/TiO$_2$, and m-SiO$_2$)

and nanocrystalline titanium dioxide shell. The developed route is versatile and convenient for the preparation of this material in gram quantities. Their photocatalytic activity was investigated by looking at the efficiency of phenol decomposition and hydrogen generation of this novel material. Our data showed a clear enhancement of photoactivity in both reactions as compared to commercial TiO$_2$-Degussa P25 catalyst. The results are encouraging and justify the need for further studies with the developed m-SiO$_2$/TiO$_2$.

Conclusions

In summary, we have successfully fabricated uniform core/shell structures with a mesoporous silica core

References

Bian SW, Ma Z, Zhang LS, Niu F, Song WG (2009) Silica nanotubes with mesoporous walls and various internal

morphologies using hard/soft dual templates. Chem Comm 14:1261–1263

Chen SL (1998) Preparation of monosize silica spheres and their crystalline stack. Physicochem Eng Asp 142:59–63

Chen HM, He JH, Tang HM, Yan CX (2008) Porous silica nanocapsules and nanospheres: dynamic self-assembly synthesis and application in controlled release. Chem Mater 20:5894–5900

Das DP, Parida KM, Mishra BK (2007) A study on the structural properties of mesoporous silica spheres. Mater Lett 61:3942–3945

Deng X, Yue Y, Gao Z (2002) Gas-phase photo-oxidation of organic compounds over nanosized TiO_2 photocatalysts by various preparations. Appl Catal 39:135–147

Deng YH, Qi DW, Deng CH, Zhang XM, Zhao DY (2008) Superparamagnetic high-magnetization microspheres with an $Fe_3O_4 \cdot SiO_2$ core and perpendicularly aligned mesoporous SiO_2 shell for removal of microcystins. J Am Chem Soc 130:28–29

Fei HL, Liu YP, Li YP, Sun PC, Yuan ZZ, Li BH, Ding DT, Chen TH (2007) Selective synthesis of borated meso-macroporous and mesoporous spherical TiO_2 with high photocatalytic activity. Micropor Mesopor Mater 102: 318–324

Fujishima A, Honda K (1972) Electrochemical photolysis of water at a semiconductor electrode. Nature 238:37–38

Jia BP, Gao L, Sun J (2007) Self-assembly of magnetite beads along multiwalled carbon nanotubes via a simple hydrothermal process. Carbon 45:1476–1481

Kingam KJ, Hemley RJ (1994) Raman spectroscopic study of microcrystalline silica. Am Miner 79:269–273

Kim W, Suh DJ, Park TJ, Hong IK (2007) Photocatalytic degradation of methanol on titania and titania-silica aerogels prepared by non-alkoxide sol–gel route. Top Catal 44:499–505

Le Y, Pu M, Chen J (2007) Theoretical and experimental studies on the silica hollow spheres. J Non-Cryst Solids 353:164–169

Lee YG, Park JH, Oh C, Oh SG, Kim YC (2007) Preparation of highly monodispersed hybrid silica spheres using a one-step sol−gel reaction in aqueous solution. Langmuir 23:10875–10878

Li M, Hong Z, Fang Y, Huang F (2008) Synergistic effect of two surface complexes in enhancing visible-light photocatalytic activity of titanium dioxide. Mater Res Bull 43:2179–2186

Lim SH, Phonthammachai N, Pramana SS, White TJ (2008) Robust gold-decorated silica−titania pebbles for low-temperature CO catalytic oxidation. Langmuir 24:6226–6231

Long R, Dai Y, Huang B (2009) Structural and electronic properties of iodine-doped anatase and rutile TiO_2. Comput Mater Sci 45:223–228

Muruganandham M, Swaminathan M (2006) Photocatalytic decolourisation and degradation of reactive orange 4 by TiO_2-UV process. Dyes Pigmen 68:133–142

Park JH, Kim S, Bard AJ (2006) Novel carbon-doped TiO_2 nanotube arrays with high aspect ratios for efficient solar water splitting. Nano Lett 6:24–28

Park MVDZ, Annema W, Salvati A, Lesniak A, Elsaesser A, Barnes C, McKerr G, Howard CY, Lynch I, Dawson KA, Piersma AH, Jong WH (2009) In vitro developmental toxicity test detects inhibition of stem cell differentiation by silica nanoparticles. Toxicol Appl Pharmacol 240:108–116

Stober W, Fink A, Bohn EJ (1968) Controlled growth of monodisperse silica spheres in the micron size range. Colloid Interface Sci 26:62–69

Tan LK, Kumar MK, An WW, Gao H (2010) Transparent, well-aligned TiO_2 nanotube arrays with controllable dimensions on glass substrates for photocatalytic applications. Am Chem Soc Appl Mater Interfaces 2:498–503

Tian G, Dong L, Wei C, Huang J, He H, Shao J (2006) Investigation on microstructure and optical properties of titanium dioxide coatings annealed at various temperature. Opt Mater 28:1058–1063

Wan L, Li JF, Feng JY, Sunb W, Mao ZQ (2007) Anatase TiO_2 films with 2.2 eV band gap prepared by micro-arc oxidation. Mater Sci Eng 139:216–220

Yang LM, Wang Y, Luo GS, Dai YY (2008) Preparation and functionalization of mesoporous silica spheres as packing materials for HPLC. Particuology 6:143–148

Yu H, Yu J, Cheng B (2007) Photocatalytic activity of the calcined H-titanate nanowires for photocatalytic oxidation of acetone in air. Chemosphere 66:2050–2057

Zhang J, Post M, Veres T, Jakubek ZJ, Guan J, Wang DS, Normandin F, Deslandes Y, Simard B (2006) Laser-assisted synthesis of superparamagnetic Fe·Au core−shell nanoparticles. J Phys Chem 110:7122–7128

Zhang H, Zhong X, Xu JJ, Chen HY (2008) Fe_3O_4/Polypyrrole/Au nanocomposites with core/shell/shell structure: synthesis, characterization, and their electrochemical properties. Langmuir 24:13748–13752

Zhu YF, Fang Y, Kaskel S (2010) Folate-conjugated $Fe_3O_4 \cdot SiO_2$ hollow mesoporous spheres for targeted anticancer drug delivery. J Phys Chem 114:16382–16388

Zielińska B, Borowiak-Palen E, Kalenczuk RJ (2011) Preparation, characterization and photocatalytic activity of metal-loaded $NaNbO_3$. J Phys Chem Solids 72:117–123